Journal of Micromechanics and Microengineering

PAPER • OPEN ACCESS

Controlling adhesion between multi-asperity contacting surfaces in MEMS devices by local heating

To cite this article: A Gkouzou *et al* 2016 *J. Micromech. Microeng.* **26** 095020

View the article online for updates and enhancements.

You may also like

- Cavity-enhanced sacrificial layer micromachining for faster release of thin film encapsulated MEMS
Jae-Wung Lee, Jaibir Sharma, Margarita Sofia Narducci et al.
- Integration of AlN with molybdenum electrodes and sacrificial amorphous silicon release using XeF_2
Jaibir Sharma, Sanchitha Fernando and Wee Ming Tan
- Vibrational communication system in ultrasonic frequency band
R. Takasawa and S. Nagasawa

This content was downloaded from IP address 202.8.112.230 on 09/06/2023 at 05:42

OPEN ACCESS
IOP Publishing
Journal of Micromechanics and Microengineering
J. Micromech. Microeng. **26** (2016) 095020 (13pp)
doi:10.1088/0960-1317/26/9/095020

Controlling adhesion between multi-asperity contacting surfaces in MEMS devices by local heating

A Gkouzou[1], J Kokorian[1], G C A M Janssen[1] and W M van Spengen[1,2]

[1] Delft University of Technology, Department of Precision and Microsystems Engineering, Mekelweg 2, 2628 CD Delft, The Netherlands
[2] Falco Systems BV, Van Boshuizenstraat 12, 1083 BA Amsterdam, The Netherlands

E-mail: a.gkouzou@tudelft.nl

Received 10 December 2015, revised 14 February 2016
Accepted for publication 6 April 2016
Published 4 August 2016

Abstract
In this work, we have incorporated heaters in a MEMS device, which allow the *in situ* local heating of its contacting surfaces. This design offers a promising solution for MEMS devices with contacting components by preventing capillary-induced adhesion. The force of adhesion was assessed by optically measuring in-plane snap-off displacements. We were able to decrease adhesion from 500 nN to 200 nN with just one heated surface of which the temperature was set above 300 °C. The temperature should not be set too high: we observed increased adhesion due to a direct bonding process once the temperature was increased above 750 °C. Remarkably, adhesion increased by heating from room temperature to 75 °C, which is attributed to more water being transferred to the contact area due to faster kinetics. We observed the same effect in the cases where both surfaces were heated, although at slightly different temperatures. We demonstrated that heating only one surface to between 300 °C and 750 °C is sufficient to significantly lower adhesion, due to the removal of capillary menisci. The required heater is typically most easily implemented in a stationary part of the device.

Keywords: MEMS device, adhesion, stiction, displacement, temperature, micro-Raman spectroscopy, capillary condensation

(Some figures may appear in colour only in the online journal)

1. Introduction

Micro-electromechanical systems or MEMS are microscale devices that are used in a wide range of applications in our daily lives. They can be found e.g. in biomedical [1], automotive and aerospace [2], communications [3], and power and energy [4] applications. At present, MEMS have typically been designed in such a way that their components mostly avoid contact. The reason behind this is to minimize the likelihood of stiction between two surfaces. Stiction is caused by adhesion, and it is fatal for many MEMS devices with contacting surfaces.

Adhesion is the combined effect of all surface forces including, but not limited to, capillary, electrostatic and van der Waals forces, as well as forces caused by solid bridging, hydrogen bonding and asperity-to-asperity nano-welding [5, 6]. These surface forces are usually attractive and become important when the surface-to-volume ratio is large, which is the case in MEMS devices. The capillary force dominates the other adhesion forces between hydrophilic surfaces in all but the driest environments. When two surfaces are close enough, water condenses around the contact area forming a capillary meniscus [7], an effect known as capillary-induced adhesion. This gives rise to an attractive capillary force that must be overcome to separate the surfaces.

Original content from this work may be used under the terms of the Creative Commons Attribution 3.0 licence. Any further distribution of this work must maintain attribution to the author(s) and the title of the work, journal citation and DOI.

For the past 30 years, the MEMS industry has managed to build many reliable devices by avoiding contacting surfaces. However, in some cases, a MEMS device may consist of microstructures that are intentionally forced to contact the substrate or other microstructures. Such components involve scanning MEMS mirrors [8], deformable grating light modulators [9], and impact microactuators [10], as well as micro gears and turbines. After repetitive contact, the surfaces in these structures are often observed to adhere permanently to each other. In some other cases, stiction occurs accidentally, especially when suspended elements are involved. In addition, the surface properties can be particularly unpredictable when the environmental conditions are not tightly controlled. Thus, devices that include cantilevers, suspended proof masses, gyroscopes, RF resonators and oscillators are likely to exhibit stiction phenomena. It is therefore of paramount importance to address and overcome the adhesion-related issues.

Traditionally, the research and development conducted to minimize adhesion between contacting surfaces in MEMS devices can be classified in two categories. One category involves the mechanical modification of surfaces in order to minimize the real contact area, for example, through the increase of surface roughness [11] or by applying micro-dimples [12]. The other focuses on the chemical modification of the contacting surfaces. This is realized by hydrogen termination [13], chemical vapour deposition of anti-stiction coatings such as self-assembled monolayers (SAMs) [14], deposition of hard coatings like diamond-like carbon (DLC) [15], or even by using a completely different structural material, like ultrananocrystalline diamond [16]. The approaches involving the mechanical modification of surface topography solve the problem of adhesion only partially, and they are mainly used to tackle release stiction that may occur during the drying process in microfabrication [17]. Hydrogen termination provides an unstable interface [18]. SAMs, as the term indicates, are limited to a single monolayer. This monolayer can be non-uniform, prone to wear and unable to tolerate high temperatures [19]. Finally, DLC coatings often suffer from delamination from the structural elements of the MEMS device and typically introduce high stress gradients in the structural elements [20]. Thus, much work remains to be done to find (in)organic, tough coatings that can be used as lubricating layers and also as adhesion prevention in MEMS contacting surfaces.

In this work, we propose the use of a new third approach, where high temperatures are generated locally at the contacting surfaces of a MEMS device. The subsequent evaporation of water will decrease capillary condensation and hence decrease adhesion. This approach mimics experiments by Greiner *et al*, in which they explore the dependence of nanoscale friction on contact temperature [21]. In their work, a heated atomic force microscope (AFM) tip was slid against a silicon oxide substrate in a humid environment. It was shown that for tip temperatures of 75 °C friction increases to a maximum, an effect ascribed to more fully developed capillary menisci between the tip and the substrate at this temperature. Furthermore, friction decreases significantly and remains low above 100 °C, due to the evaporation of water from the contact. Pull-off experiments performed with the same tip to study adhesion demonstrated similar behaviour.

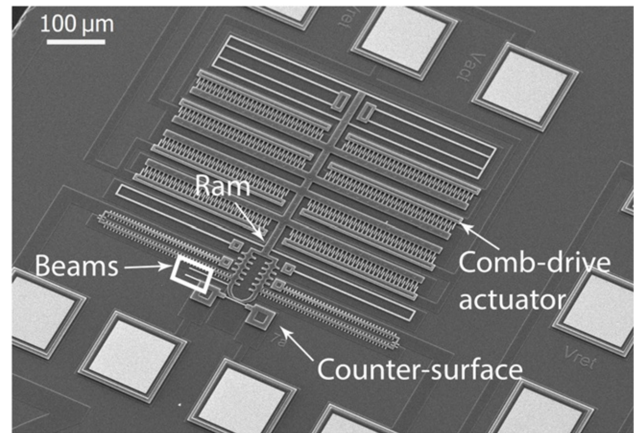

Figure 1. SEM micrograph of the adhesion sensor. Comb-drive actuators push the ‘ram’ forward until it touches the counter-surface. The beams, one attached to the ram and the other stationary, are used for measuring the motion of the ram.

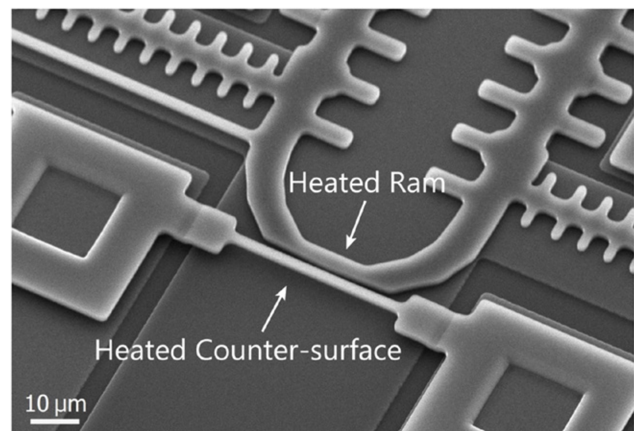

Figure 2. SEM micrograph zoomed in at the contact area. Through the thin parts of the ram and the counter-surface, the contact area is selectively heated. Water is expected to evaporate, reducing adhesion.

For our study, we have developed a new concept of a MEMS device with integrated micro-heaters that allow the *in situ* selective increase of temperature only where contact occurs and locally remove condensed water. Contrary to the case of Greiner *et al*, in our study we are dealing with a multi-asperity contact, which is more relevant to the MEMS scale than the investigation of a single- or few-asperity contact of an AFM. Adhesion in MEMS devices is best studied with a MEMS test device. It is our goal to obtain an understanding of adhesion on the microscale and, based on this knowledge, to reduce and eventually solve the stiction problems that currently hamper the MEMS industry.

2. Device design and actuation

To carry out our study, we have designed an adhesion sensor that is based on the ‘nano-battering ram’ by van Spengen

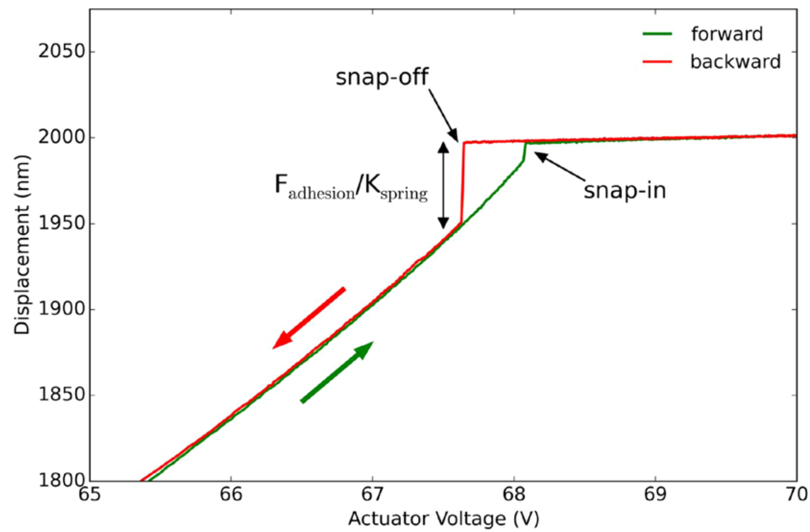

Figure 3. An example of a displacement measurement of the ram as a function of the actuator voltage. With increasing actuator voltage, the ram is moving forward until it makes contact with the counter-surface, where snap-in occurs. Upon decreasing the voltage, the ram remains in contact with the counter-surface until it is released during the backward motion. The snap-off length is a measure of the force of adhesion.

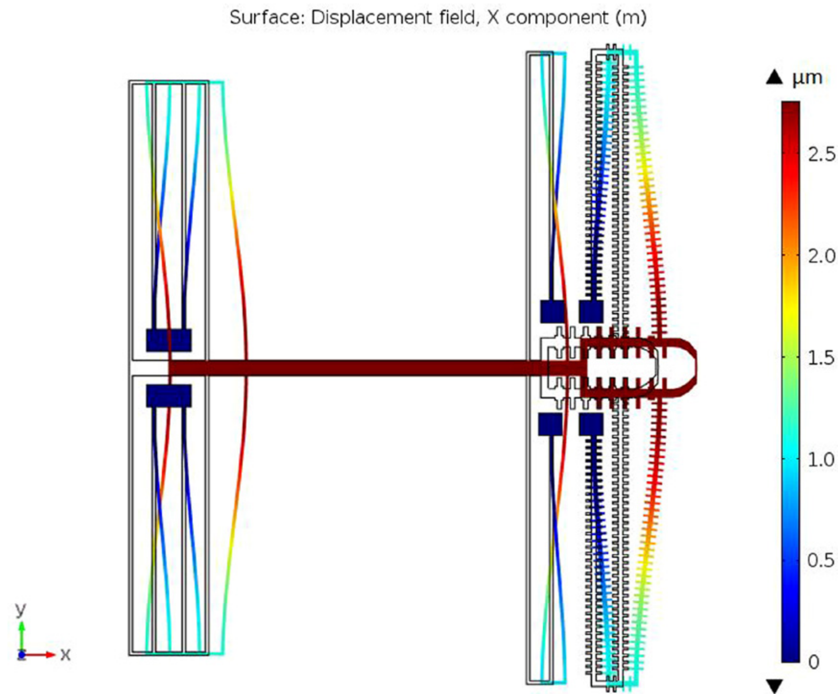

Figure 4. Simulated device deformation at the ram's maximum displacement of 2.76 μm. The displayed colour is proportional to the displacement.

et al [22]. It is manufactured in a three-layer polycrystalline silicon multi-user MEMS process by MEMSCAP Inc., commercially known as PolyMUMPs™. Figure 1 shows a scanning electron microscope (SEM) micrograph of the adhesion sensor and figure 2 illustrates a close-up of the contacting parts. The device consists of a comb-drive actuator and a 'ram' that can move over a distance of 2 μm before it touches a counter-surface. When the actuator voltage is increased, the ram moves forward until its head makes contact with the counter-surface (snap-in) and temporarily adheres to it. When the voltage is reduced again, the head of the ram remains stuck until the restoring spring forces are large enough to pull it from the counter-surface (snap-off). The displacement of the ram after snap-off is a measure for the adhesion force. By passing an electrical current through the thin parts of the ram and the counter-surface, the device is heated *in situ* at the area where contact occurs.

To measure the force of adhesion, we use an optical method for detecting in-plane displacements with sub-nm resolution developed by Kokorian *et al* [23]. For each voltage applied on the comb-drive actuators, an image of

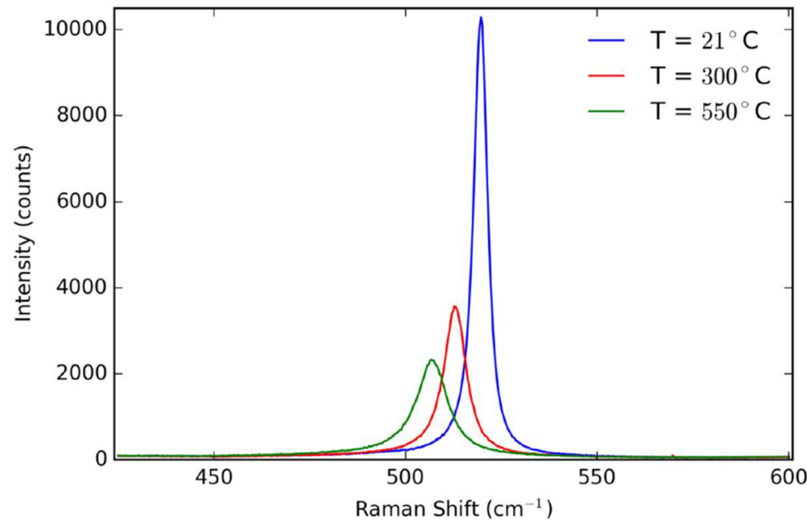

Figure 5. Raman spectra of polycrystalline silicon at three different temperatures. The position of the peak (519 cm^{-1} at room temperature) changes with temperature, and hence it can be used for the calibration between heater voltage and heater temperature.

two beams, one stationary and one attached to the moving ram, is captured by a standard optical microscope, and the displacement is determined through an algorithm based on curve-fitting. Figure 3 demonstrates a measurement of the displacement of the ram as a function of the voltage applied to the comb-drive actuators connected to it. The adhesion force is equal to the difference between the restoring spring force just before the ram's snap-off from the counter-surface and the restoring spring force after snap-off. Adhesion can be calculated from the voltage–displacement curve by multiplying the snap-off jump length with the spring constant of the support springs.

The spring constant of the ram was computed numerically via finite element analysis (FEA) using COMSOL Multiphysics 4.3b (figure 4). A 2D solid mechanics model was developed to calculate the maximum displacement of the moving component, from which it was possible to extract the stiffness of the support springs connected to it. A 10 μN load was applied onto the ram in the *x*-axis direction. The material properties of polycrystalline silicon used in the computation were a Young's Modulus of 169 GPa and Poisson's ratio of 0.22 [24]. The resulting displacement was 2.76 μm, which corresponds to a spring constant of 3.6 N m^{-1}.

3. Calibration between heater voltage and heater temperature

The contact area between the ram and the counter-surface is heated *in situ* by applying a voltage to their heating elements. The heaters subsequently convert the corresponding electrical power to heat, which relates to a certain temperature. It is possible to determine this temperature very locally using micro-Raman spectroscopy.

Micro-Raman spectroscopy offers the possibility of assessing the local temperature with μm resolution, limited by the spot size of the focused laser light that is used to excite the material. Higher temperatures increase the lattice spacing due to thermal expansion, and they increase the vibrational mode frequencies of the silicon lattice [25]. By observing the Raman peak position while changing the temperature of the polycrystalline silicon, we are able to obtain the relation between heater voltage and the temperature of the heated parts and locally map the temperature of the contact area.

The Raman spectra were obtained on a HORIBA Scientific LabRam HR spectrometer with excitation from an Argon-ion laser with a 514 nm wavelength, and a 50× objective lens with a numerical aperture of 0.5. We first placed the device on a heating stage to set the sample temperature and obtain the Raman peak position of polycrystalline silicon for a range of temperatures. In figure 5, the spectra that correspond to room temperature, 300 °C and 550 °C are plotted. The Raman peak positions of each sample temperature, interpolated by a linear curve fit, are shown in figure 6. Afterwards, we applied a range of voltages to the heating element of the counter-surface. Because of the small lateral dimension of the counter-surface, we observed two peaks in the Raman spectra, one of which corresponds to the Raman signal of the substrate (figure 7). The Raman peak position of the substrate does not shift with the increase of the heater voltage, therefore we are able to distinguish the Raman signal of the substrate from the one of the device layer. The Raman peak position of the device layer is the one we use in our calibration. Having determined all Raman peak positions for the range of heater voltages, we were able, through figure 6, to relate the heater voltage to the local heater temperature of the counter-surface (figure 8). A quartic (fourth-degree) polynomial curve fit was used to interpolate the data points. The calibration between heater voltage and temperature for the heating element of the ram was performed in the same way as for the counter-surface (figure 9).

Furthermore, we have investigated whether the heating of either the ram or the counter-surface would cause heating of the other component through thermal conduction. We

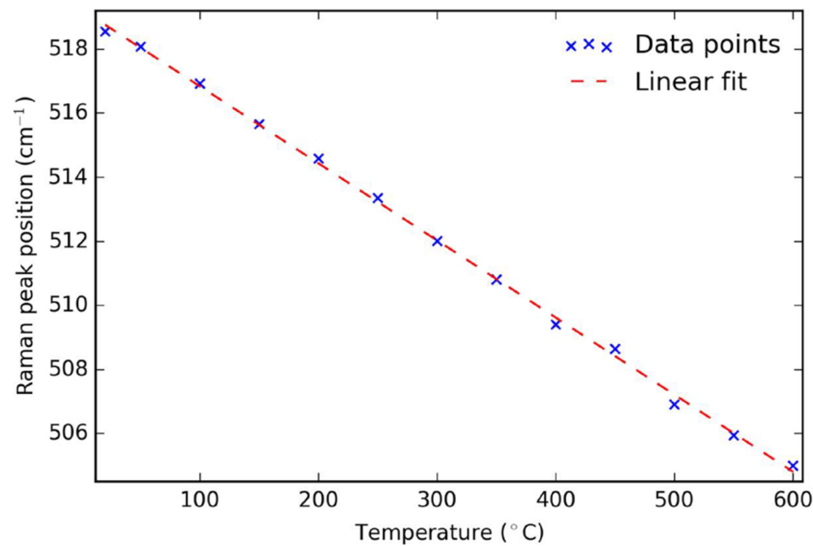

Figure 6. Calibration curve of the Raman peak position measured using the heating stage. A linear curve fit was used to interpolate the data points. Because the Raman peak position is a function of temperature, this curve can be used to relate heater voltage to local heater temperature.

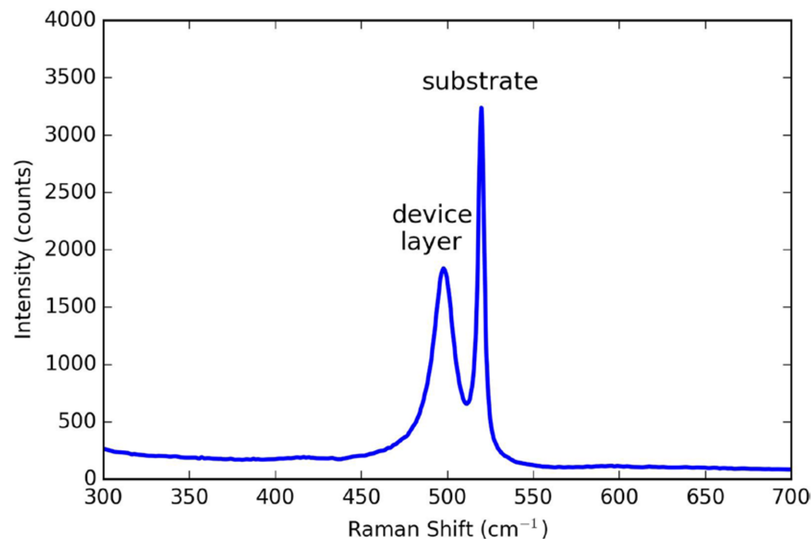

Figure 7. Raman spectrum of the counter-surface at a heater voltage of 5 V. Observe the two Raman signals that originate from both the substrate and the device layer. In our calibration, we use the Raman peak position that corresponds to the device layer.

measured the temperature of the counter-surface while in contact with the ram, when the latter was set to a $T_{ram,set}$ of room temperature, 30 °C and 50 °C. These temperatures correspond to the temperatures the ram would have had if it had been out of contact from the counter-surface, set to room temperature. The heater temperature of the counter-surface was swept from room temperature to 955 °C. We observed that the heater temperature of ram, $T_{ram,set}$, has very little influence on the temperature of the counter-surface. On the contrary, the heater temperature of the counter-surface, which we will simply refer to as temperature of the counter-surface, greatly influences the temperature of the ram, regardless of the ram heater temperature, $T_{ram,set}$. This is due to the fact that the thermal resistance to the substrate is much smaller for the counter-surface than for the ram, as the latter has long springs connected to it. The temperature of the ram for a given temperature of the counter-surface, for example 400 °C, is 330 °C, 365 °C and 380 °C, for each of the three different $T_{ram,set}$. In figure 10, we show the temperature of the ram as a function of the temperature of the counter-surface.

4. Experiments

We have studied the influence of local temperature on adhesion by performing ten consecutive cycles per temperature of one heating element, and the opposite element is either at room temperature or set to a certain temperature. In table 1, we classify the different types of experiments that are conducted in this paper. We first started with the temperature of the counter-surface swept from room temperature to 855 °C, with the temperature of the ram sweeping from room temperature to 715 °C. This experiment has a 'twin', in which the temperature of the counter-surface started at 855 °C and was swept back

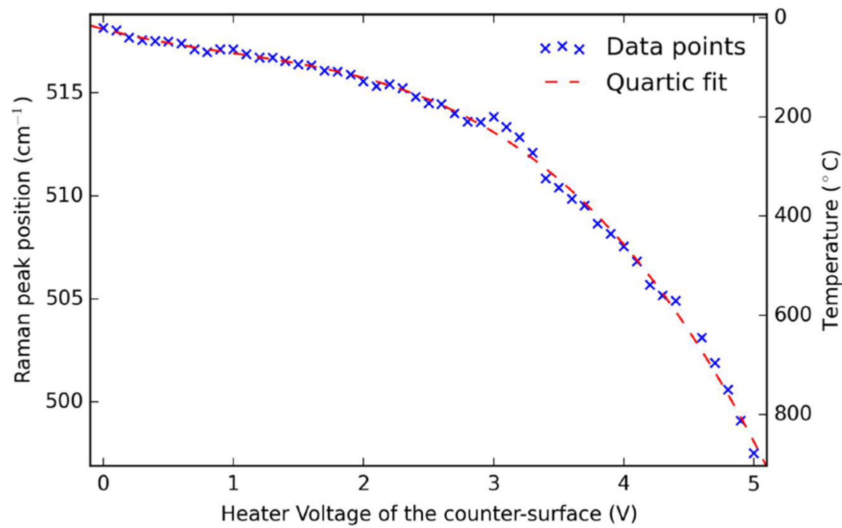

Figure 8. Raman peak position of the device layer as a function of the heater voltage applied to the heater of the counter-surface, while the ram was not in contact with the counter-surface. A quartic (fourth-degree) polynomial was used to fit the data points.

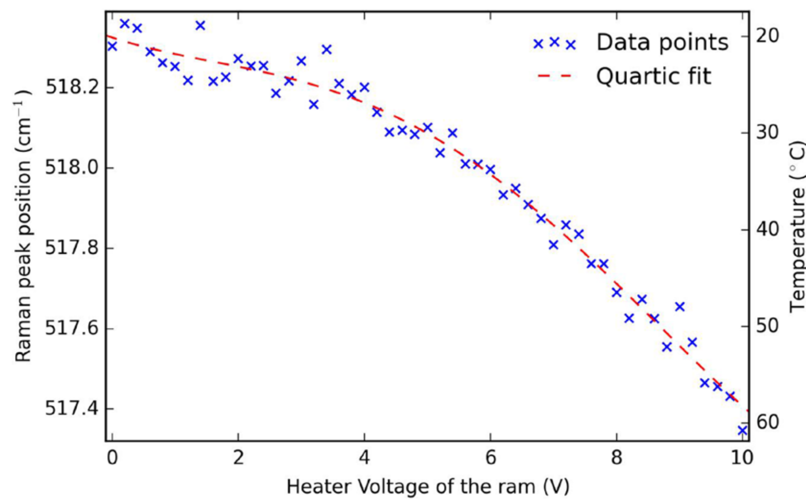

Figure 9. Raman peak position of the device layer as a function of the heater voltage applied to the heater of the ram, while the ram was not in contact with the counter-surface. A quartic (fourth-degree) polynomial was used to fit the data points.

to room temperature. We carried out such an experiment because we are also interested in investigating whether elevated temperatures from the beginning of the experiment trigger different effects between the contact area and hence result in different adhesion values.

We observed that, when the temperature of the counter-surface was set above 400 °C, the adhesion values were very low. Therefore, we performed another experiment in which we swept the heater temperature of the ram from room temperature to 60 °C, while the temperature of the counter-surface was set to 400 °C. In fact, the temperature of the ram ranged from 25 °C to 70 °C when not in contact with the counter-surface, and, once in contact, the temperature ranged from 330 °C to 385 °C. Above 385 °C, the ram was seen to behave erratically: the support springs buckle due to the unintended thermal expansion and push it into the substrate. This leads to a stick-slip motion that prevents us from measuring adhesion. Therefore, the temperature of the ram had to be kept below 385 °C. This experiment was sufficient to reveal two contact temperatures of the ram, 365 °C and 380 °C, at which adhesion increased and decreased respectively. These two temperatures correspond to ram heater temperatures of 30 °C and 50 °C, with the counter-surface kept at room temperature, and subsequently reached temperatures of 725 °C and 740 °C when the temperature of the counter-surface was set to 855 °C. These temperatures were used for two twin experiments, with the temperature of the counter-surface starting from room temperature to 855 °C, and from 855 °C to room temperature.

In the following figures, we plot the force of adhesion as a function of temperature of the heating element of which the temperature was swept. The resulting adhesion force was calculated from the spring constant of the ram multiplied by the displacement measured from ten consecutive cycles. The error bars that appear in the following figures do not indicate measurement errors, but the standard deviation of the ten measured adhesion forces. This is a measure for the cycle-to-cycle variability of the adhesion force.

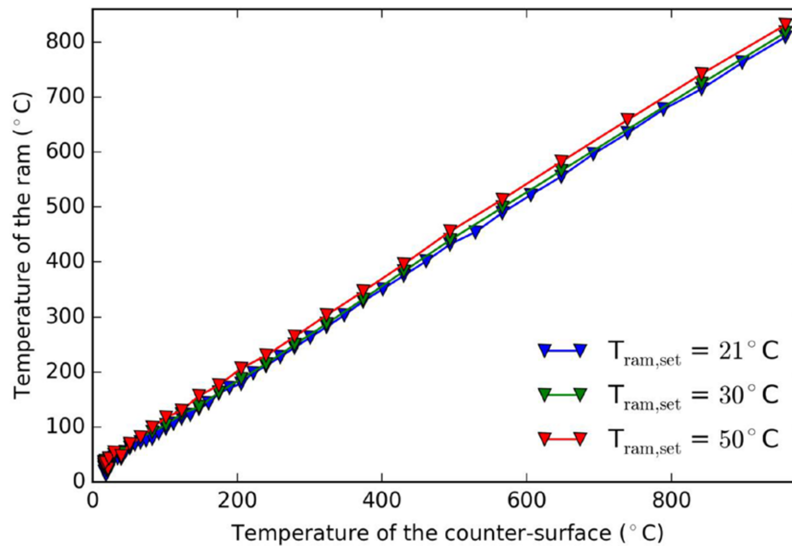

Figure 10. The temperature of the ram as a function of the temperature of the counter-surface. For different ram heater temperatures, $T_{ram,set}$, the temperatures of the counter-surface are almost the same. The temperature of the ram however is heavily dependent on the power dissipated when the element of the counter-surface is heated. The temperature $T_{ram,set}$ that is shown in the legend corresponds to the temperature the ram would have had if it had not been in contact with the counter-surface, and the counter-surface would have been at room temperature.

Table 1. An overview of the types of experiments performed with their corresponding figure numbers.

Name of the experiment	Temperature of the counter-surface	Temperature of the ram	Number of figure
A1	From room temperature to 855 °C	From room temperature to 715 °C	11
A2	From 855 °C to room temperature	From 715 °C to room temperature	12
B	400 °C	From 330 °C to 385 °C	13
C1	From room temperature to 855 °C	From 30 °C to 725 °C	14
C2	From 855 °C to room temperature	From 725 °C to 30 °C	15
D1	From room temperature to 855 °C	From 50 °C to 740 °C	16
D2	From 855 °C to room temperature	From 740 °C to 50 °C	17

The temperatures of the ram given in this table are the temperatures the ram would have had if it had been in contact with the counter-surface, which is set to certain heater temperatures.

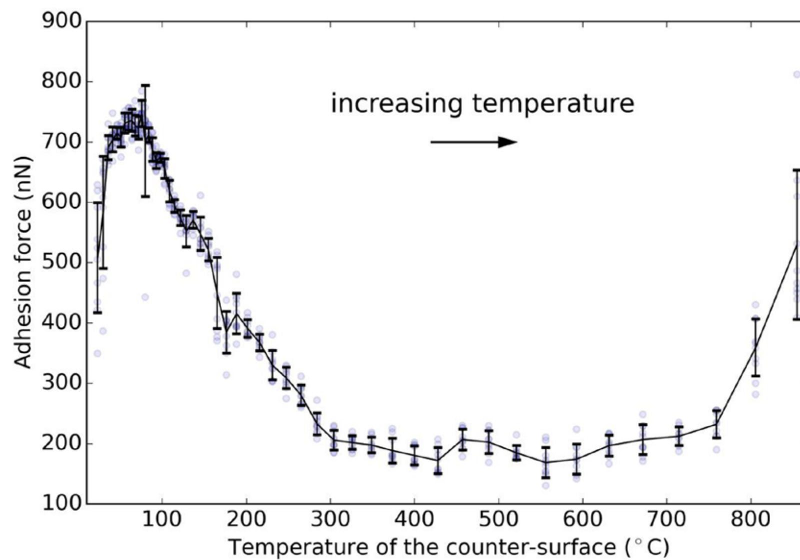

Figure 11. Adhesion evolution in experiment A1 for temperatures of the counter-surface that increased from room temperature to 855 °C. The ram was set to room temperature, but it reached a temperature of 715 °C upon contact due to the temperature of the counter-surface. The ambient temperature was between 20 °C and 21 °C, while the relative humidity was between 37.5% and 39%.

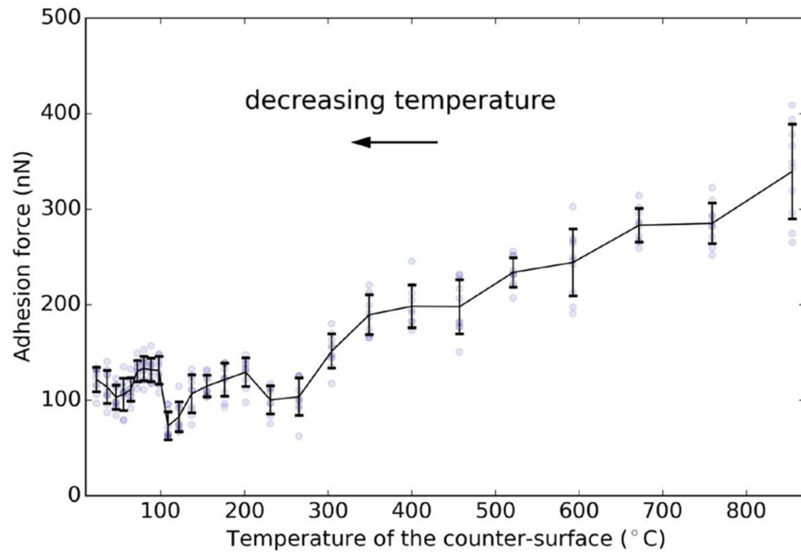

Figure 12. Adhesion evolution in experiment A2 for temperatures of the counter-surface that decreased from 855 °C to room temperature. The temperature of the ram upon contact reached 715 °C at the start of the experiment due to the temperature of the counter-surface, and it decreased back to room temperature together with the counter-surface. The ambient temperature was between 21 °C and 22 °C, while the relative humidity was between 38% and 40%.

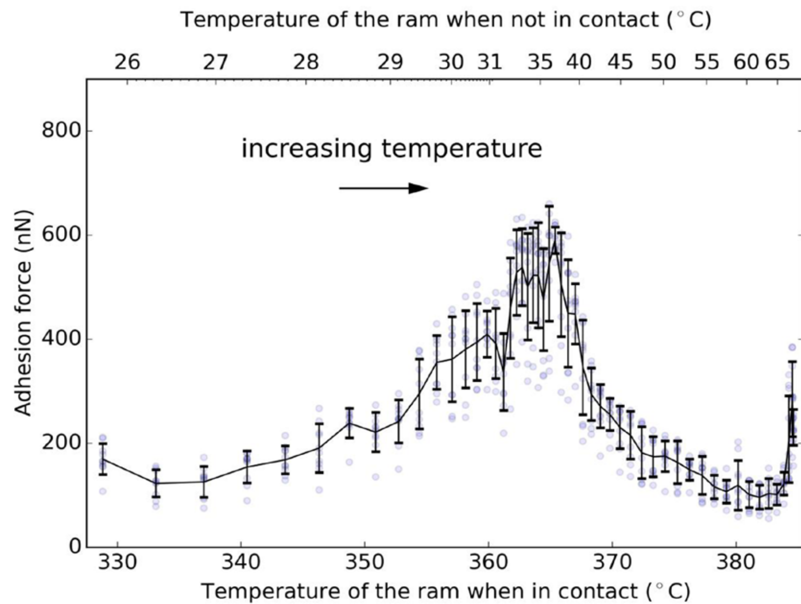

Figure 13. Adhesion evolution in experiment B for temperatures of the ram that increased from 330 °C to 385 °C, while the temperature of the counter-surface was kept at 400 °C. At the start of every ten adhesion cycles, the ram is 2 μm away from the hot counter-surface. The temperatures of the ram on the top *x*-axis will increase once it starts approaching the counter-surface. The temperatures on the bottom *x*-axis represent those the ram will reach once in contact with the counter-surface. The temperature of the ram when not in contact with the counter-surface does not have a linear relation with that of the ram when in contact with the counter-surface. The ambient temperature and the relative humidity are not known.

5. Results

For experiment A1, we swept the temperature of the counter-surface from room temperature to 855 °C. The temperature of the ram was then ranged from room temperature to 715 °C. Figure 11 shows the evolution of adhesion as a function of the temperature of the counter-surface. Adhesion reached a maximum between room temperature and 130 °C, with the highest value appearing at 75 °C. Afterwards, adhesion is seen to decrease and stabilize. It is observed that, between 300 °C and 750 °C, the adhesion force is one third of its initial value at room temperature. However, at elevated temperatures between 750 °C and 855 °C, adhesion starts to increase again.

In experiment A2, we swept the temperature of the counter-surface from 855 °C back to room temperature (figure 12). In the beginning, adhesion is very high, and gradually decreases with the decrease of the temperature of the counter-surface. This behaviour is followed by consecutive regimes, in each of which adhesion goes through a local maximum, first between 230 °C and 115 °C and

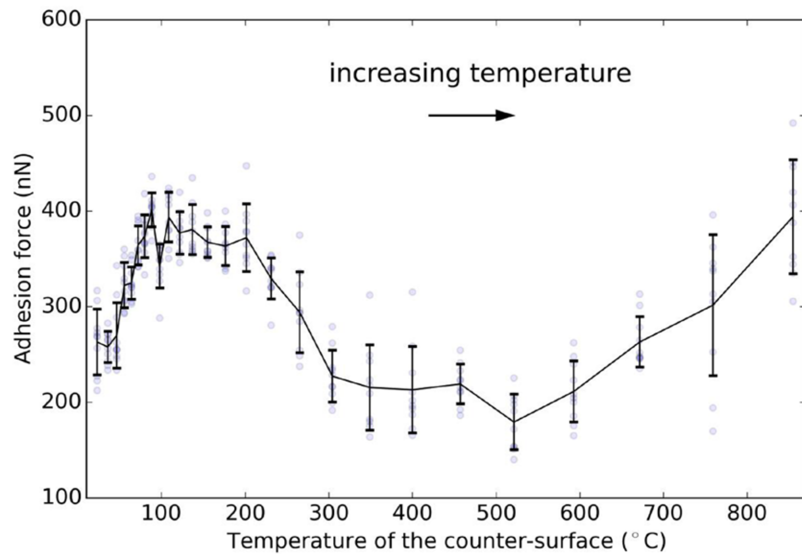

Figure 14. Adhesion evolution in experiment C1 for temperatures of the counter-surface that increased from room temperature to 855 °C. The ram was set to 30 °C, but it reached a maximum temperature of 725 °C due to the temperature of the counter-surface. The ambient temperature was between 20 °C and 20.5 °C, while the relative humidity was between 35% and 36.5%.

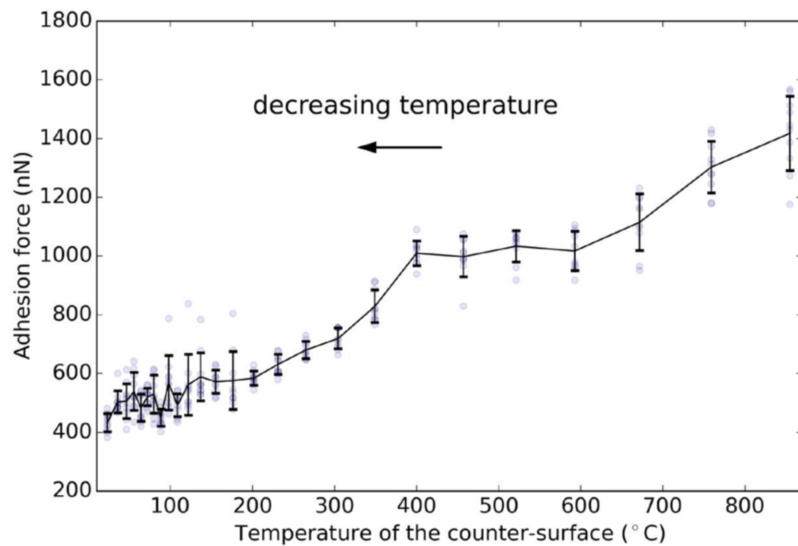

Figure 15. Adhesion evolution in experiment C2 for temperatures of the counter-surface that decreased from 855 °C to room temperature. The temperature of the ram reached 725 °C due to the temperature of the counter-surface and decreased with it to 30 °C. The ambient temperature was at 20.5 °C, while the relative humidity was between 36.5% and 42.5%.

then between 105 °C and 70 °C. From 55 °C down to room temperature, adhesion remains relatively stable.

For experiment B, we set the temperature of the counter-surface to 400 °C and swept that of the ram from 330 °C to 385 °C (figure 13). The adhesion values began relatively low, however they increased until a certain plateau for temperatures of the ram between 360 °C and 370 °C. This plateau is at a lower adhesion value than when only one surface was heated as in experiment A1, but it is still very significant. Moreover, once the temperature of the ram reached higher temperatures, adhesion decreased and became lower than when the ram was at room temperature. For temperatures of the ram between 380 °C and 385 °C, adhesion increased slightly. The temperatures of the ram on the top x-axis represent those the ram has at the beginning of each ten adhesion cycles, when it is 2 μm away from the hot counter-surface.

Because in experiment B we observed a maximum of adhesion when the temperature of the ram was at 365 °C, we carried out experiment C1 with the heater temperature of the ram set to 30 °C and the temperature of the counter-surface swept from room temperature to 855 °C (figure 14). The actual temperature of the ram was therefore ranged from 30 °C to 725 °C accordingly. Adhesion appears to increase between 50 °C and 200 °C, while, with the increase of the temperature of the counter-surface, it decreases until 520 °C, followed by a rather sudden increase of its values.

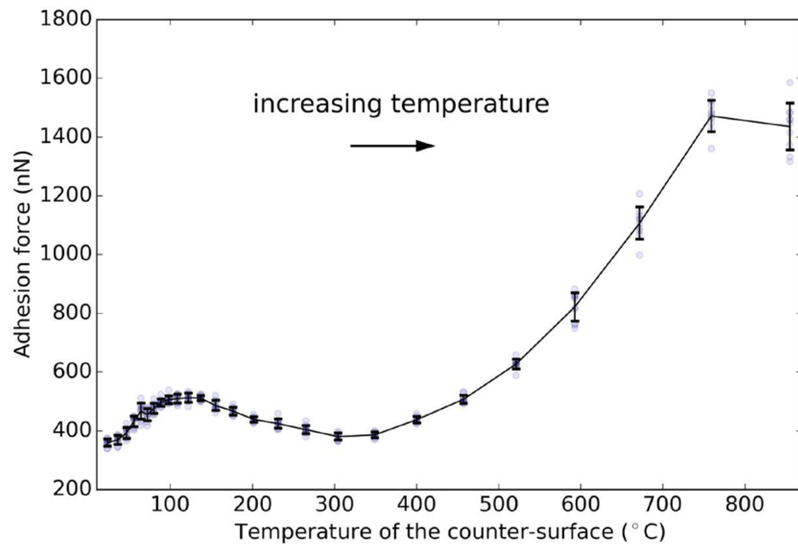

Figure 16. Adhesion evolution in experiment D1 for temperatures of the counter-surface that increased from room temperature to 855 °C. The ram was set to 50 °C, however it reached a maximum temperature of 740 °C due to the temperature of the counter-surface. The ambient temperature was between 20.5 °C and 21 °C, while the relative humidity was between 47.5% and 51.5%.

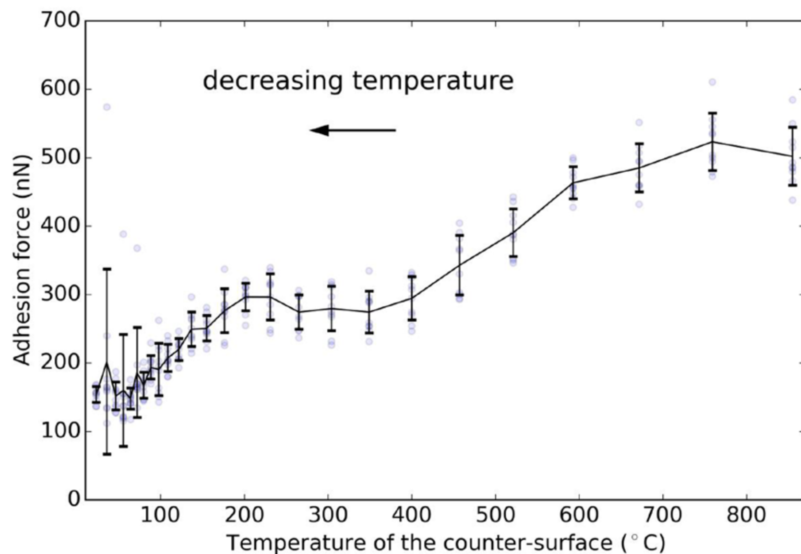

Figure 17. Adhesion evolution in experiment D2 for temperatures of the counter-surface that decreased from 855 °C to room temperature. The temperature of the ram reached 740 °C due to the temperature of the counter-surface and decreased with it to 50 °C. The ambient temperature was between 20.5 °C and 21 °C, while the relative humidity was between 39% and 41.5%.

For experiment C2, we kept the heater temperature of the ram at 30 °C, while the temperature of the counter-surface started at 855 °C, and then it was gradually set back to room temperature (figure 15). The adhesion values were particularly high in the beginning and, with the decreasing temperature of the counter-surface, they appear to stabilize between 595 °C and 400 °C. Afterwards, there is a further decrease from 350 °C to 80 °C and, from this point to room temperature, adhesion appears to obtain its lowest values.

In experiment B, the lowest value of the adhesion force was observed when the temperature of the ram was at 380 °C. Therefore, for experiment D1, we set the heater temperature of the ram to 50 °C and repeated the ten-cycle adhesion measurements by sweeping the temperature of the counter-surface from room temperature to 855 °C (figure 16). The actual temperature of the ram therefore ranged from 50 °C to 740 °C. Adhesion demonstrates a maximum between 50 °C and 155 °C. Between 155 °C and 350 °C, adhesion decreases again. From 350 °C to 855 °C, adhesion increases considerably, to about four times its value at the start of the experiment.

In experiment D2, we swept the temperature of the counter-surface from 855 °C back to room temperature, while the heater temperature of the ram was kept at 50 °C (figure 17). Adhesion was relatively high in the beginning and, with decreasing temperature of the counter-surface, it stabilized between 455 °C and 230 °C. Afterwards, there is a further decrease between 200 °C and 85 °C. From this point onwards, the mean value of adhesion seems to decrease, although it becomes highly variable from cycle to cycle.

6. Discussion

From experiments A1, C1 and D1 we are able to conclude that adhesion is low for temperatures of the counter-surface above 300 °C. This is logical due to the absence of capillary menisci, which obeys the thermodynamics of evaporation. However, it is not *a priori* clear why a local maximum in the adhesion occurs at 75 °C, 110 °C and 120 °C in each experiment respectively. This maximum can be dangerous for actual MEMS devices used at slightly elevated temperatures. For simplicity, we introduce a variable called T_{peak} to indicate all three temperatures where the local maximum is present. In addition, for temperatures of the counter-surface above 750 °C, 520 °C and 350 °C, an even higher maximum was observed. We will use the name T_{high} to represent the temperatures where very high adhesion occurs in all three experiments.

At high temperatures, thermodynamics predicts the dominance of the gas phase over the liquid phase due to the higher entropy of a gas. This explains the decrease of adhesion from T_{peak} to 300 °C. However, it does not explain the increase from room temperature to T_{peak}. We argue that this increase is due to a kinetic effect: the limited transport of water either in the adsorbed layer on the substrate or in the gas phase. With the increase in temperature, the water molecules are moving fast enough and increase their density at the contact area, which leads to larger menisci. T_{peak} is the crossover from the kinetics-dominated regime to the thermodynamics-dominated regime and will depend on the exact temperatures in the experiment, hence the different temperatures at which the peak occurs in experiments A1, C1 and D1.

The kinetics of the condensate is complicated due to the fact that the meniscus nucleation time does not only depend on the temperature but also on the transport time of the water molecules to the location where the capillary meniscus is being formed. A single voltage–displacement curve takes about 90 s to record, while the ram and counter-surface are in contact for slightly less than half of the duration of a single measurement. The contact time is then about 40 s. This time is much longer than a typical meniscus nucleation time, which is of the order of microseconds [26]. When two low-roughness multi-asperity surfaces are in contact, with the standard deviation of the height distribution of the asperities being tens of nanometers [27], they form a confined system. The path for the water to reach the contact area is smaller than the mean free path of the water vapour molecules, and the kinetics enters into a molecular flow regime. Thus, because the water molecules need time to travel to the location of the nucleating meniscus, more time is needed for an equilibrium state to be reached. This time is available only if the surfaces are in contact much longer than the normal meniscus nucleation time.

The capillary force is affected by the contact area of the condensate. The contact area can be estimated with a simple plastic flow contact mechanics model based on the bearing area concept [28]. The contact area $A_{contact}$ is expressed as the ratio of the contact force $F_{contact}$ and the effective hardness H_{eff} of the polycrystalline silicon surface. To obtain the effective hardness, all the properties of the two contacting surfaces are transferred to a single surface, while the other surface is defined to be perfectly flat and infinitely hard. The effective hardness of polycrystalline silicon is calculated as [29]:

$$H_{eff} = \frac{H_{surface} \cdot H_{surface}}{H_{surface} + H_{surface}} = \frac{H^2_{surface}}{2H_{surface}} = \frac{H_{surface}}{2} = \frac{11.0\,\text{GPa}}{2} = 5.5\,\text{GPa}.$$

The hardness $H_{surface}$ was taken to be 11.0 GPa, the mean value of 10.5 GPa and 11.5 GPa, which are the hardnesses measured by nanoindentation at two different loads and two different indentation depths [30]. The contact force $F_{contact}$ can be extracted from the voltage–displacement curve. This is done by calculating how much further the ram would have moved in the absence of the counter-surface at the maximum actuator voltage. This distance multiplied by the spring constant yields a contact force of 360 nN. The contact area $A_{contact}$ is then:

$$A_{contact} = \frac{F_{contact}}{H_{eff}} = \frac{360\,\text{nN}}{5.5\,\text{GPa}} = 65.5\,\text{nm}^2.$$

Our preliminary explanation of the high-temperature behaviour of the adhesion evolution is as follows: for temperatures of the counter-surface above T_{high}, both surfaces have been rendered sufficiently flat after repetitive contact [31]. Blunted asperities in combination with high local temperature and pressure while in intimate contact may lead to a situation known as direct bonding. The surfaces become more adhesive and the native oxide that covers them becomes more fluid-like and exhibits glassy flow. This effect is thermally activated; it is illustrative that elevated temperatures are used as a treatment step in wafer bonding processes. The temperature of both surfaces determines the starting point of this process, therefore T_{high} shifts accordingly to a lowest temperature in experiment D1, where the heater temperature of the ram is set to 50 °C.

For experiments A2, C2 and D2, in which the temperature of the counter-surface was swept from 855 °C down to room temperature, we observe higher adhesion which is indicative of the silicon-oxide bonding process as described above. The bonding process takes effect from 855 °C to T_{high}, which is equal to 265 °C, 350 °C and 455 °C for experiments A2, C2 and D2, respectively. At this moment, the two opposite surfaces form bonds with each other, and may become flatter due to the increased contact pressure. However, with the decrease of the temperature to T_{water} that corresponds to 105 °C, 90 °C and 80 °C for the three experiments, the chances of forming chemical bonds decrease significantly and so does the real contact area. The existing bonds are breaking, the surface roughness becomes higher and, in the absence of water, adhesion is mainly caused by van der Waals forces. With further decrease of the temperature from T_{water} to room temperature, water returns to the contact and forms capillary menisci which contribute to the total adhesion.

In experiments A1, C1 and D1, the absolute adhesion values vary per experiment, due to different devices being used in each experiment that all have slightly different surface roughnesses. Such differences between nominally identical devices have recently been extensively addressed theoretically [32]. Furthermore, we observe that the peak attributed

to capillary condensation is shifting towards higher temperatures of the counter-surface with higher temperatures of the ram. The reason behind this is that the temperature of the ram influences the temperature of the interface between the counter-surface and itself. We expect the temperature of the interface to be somewhere between that of the counter-surface and the ram. The way in which heat is conducted away from the heating elements once they are in contact may also influence the interface temperature. For the same temperature of the counter-surface, we observe that the temperature of the interface is lower when the ram was at room temperature, then it increases with the heater temperature of the ram at 30 °C and it goes even higher when the ram was set to 50 °C. For the regime when the direct bonding takes place, which is when higher adhesion is observed in all three experiments, the temperature is also seen to shift accordingly, and the same occurs for the twin experiments A2, C2 and D2.

For experiment B, where the temperature of the counter-surface was set to 400 °C and that of the ram was swept from 330 °C to 385 °C, a local maximum appears between 360 °C and 370 °C, probably caused by capillary condensation. However, the temperatures of the ram before it makes contact with the counter-surface are between 30 °C and 45 °C. We suggest that, while the ram is approaching the hot counter-surface, water is being evaporated from its surface just before contact occurs. The temperature shifts from 30 °C to 360 °C and from 45 °C to 370 °C, so the contact experiences the 'dangerous' temperature range where kinetic effects are more pervasive. Because two multi-asperity contacting surfaces compose a confined system, the water, which starts to evaporate once the surfaces are approaching one another, remains trapped and forms menisci at the contact area. The probability for the water to exist in the liquid state is temperature-dependent and therefore it seems that a capillary meniscus is still energetically favourable. In addition, the maximum between 360 °C and 370 °C is shifted above the boiling point of water, which was also observed in experiments C1 and D1. Therefore, the shift in temperature is consistent in all experiments where two hot contacting surfaces are involved.

7. Conclusions

In this work we have demonstrated the reduction of adhesion in MEMS devices by locally heating the contacting surfaces. The incorporated heaters allow *in situ* Joule heating of the contacting MEMS sidewalls which leads to the evaporation of adsorbed water. As revealed in our study, the optimum temperature is slightly above 100 °C. Between room temperature and 100 °C, the kinetics of water prominently increase adhesion. Care should be taken that the temperature is not set too high (above 750 °C), as there is a risk of thermally activated direct bonding of the native oxides that cover most silicon-based MEMS devices. Local heating is recommended to mitigate stiction problems in hydrophilic MEMS surfaces to keep the adhesion low and stable. However, the temperature increase should be between well-defined limits; heating only one surface to between 300 °C and 750 °C appears to be ideal. In actual MEMS designs, incorporating a heater to the stationary surface only appears to be sufficient, and is much easier to implement than designing a heater within a moving structure.

Acknowledgments

We would like to thank Evert C Hooijkamp for his help in the numerical computation with FEA and J Tijn van Omme for his help with the Raman measurements. This work is part of the research programme 'Fundamental aspects of friction' under ref. no. 129 of the Foundation for Fundamental Research on Matter (FOM), which is part of the Netherlands Organisation for Scientific Research (NWO).

References

[1] Ashraf M W, Tayyaba S and Afzulpurkar N 2011 Micro electromechanical systems (MEMS) based microfluidic devices for biomedical applications *Int. J. Mol. Sci.* **12** 3648–704

[2] Ma Z and Chen X 2009 MEMS testing and applications in automotive and aerospace industries *Proc. SPIE* **7284** 728409-1–8

[3] Tilmans H A C, de Raedt W and Beyne E 2003 MEMS for wireless communications: 'from RF-MEMS components to RF-MEMS-SiP' *J. Micromech. Microeng.* **13** S139–63

[4] Cook-Chennault K A, Thambi N and Sastry A M 2008 Powering MEMS portable devices—a review of non-regenerative and regenerative power supply systems with special emphasis on piezoelectric energy harvesting systems *Smart Mater. Struct.* **17** 043001

[5] Maboudian R and Howe R T 1997 Critical review: adhesion in surface micromechanical structures *J. Vac. Sci. Technol.* B **15** 1–20

[6] Shavezipur M, Carraro C and Maboudian R 2013 Effects of actuation methods and temperature on adhesion force between polycrystalline silicon surfaces in MEMS *Proc. SPIE* **8614** 861402-1–7

[7] Sirghi L 2012 Transport mechanisms in capillary condensation of water at a single-asperity nanoscopic contact *Langmuir* **28** 2558–66

[8] Kiang M, Solgaard O, Muller R S and Lau K Y 1996 Surface-micromachined electrostatic-comb driven scanning micromirrors for barcode scanners *MEMS' 6 (San Diego, CA, Feb. 1996)* pp 192–7

[9] Sandejas F S A, Apte R B, Banyai W C and Bloom D M 1993 Surface microfabrication of deformable grating light valves for high-resolution displays *Proc. 7th Int. Conf. on Solid-State Sensors and Actuators (Transducers 93) (Yokohama, Japan, 7–10 June, 1993)* Abstract of late news papers, pp 6–7

[10] Zhao X, Dankowicz H, Reddy C K and Nayfeh A H 2004 Modeling and simulation methodology for impact microactuators *J. Micromech. Microeng.* **14** 775–84

[11] Komvopoulos K 1996 Surface engineering and microtribology for microelectromechanical systems *Wear* **200** 305–27

[12] Zhang X-J, Dong Y-K, Liu Y-H and Schaefer J A 2009 Effect of micro-dimple patterns on capillary pull-off force and friction force of silicon surface *Chin. Phys.* B **18** 231–7

[13] Houston M R, Howe R T and Maboudian R 1997 Effect of hydrogen termination on the work of adhesion between rough polycrystalline silicon surfaces *J. Appl. Phys.* **81** 3474–83

[14] Zhuang Y X, Hansen O and He J C 2009 Growth and properties of self-assembled monolayers on metals *J. Phys. Conf. Ser.* **152** 012029
[15] Smallwood S A, Eapen K C, Patton S T and Zabinski J S 2006 Performance results of MEMS coated with a conformal DLC *Wear* **260** 1179–89
[16] Buja F, Kokorian J, Sumant A V and van Spengen W M 2015 Studies on measuring surface adhesion between sidewalls in boron doped ultrananocrystalline diamond based microelectromechanical devices *Diam. Relat. Mater.* **55** 22–31
[17] Bright V M *et al* 2004 Packaging of advanced micro- and nanosystems *Enabling Technology for MEMS and Nanodevices* ed H Baltes *et al* (Weinheim: Wiley-VCH) pp 93–164
[18] Mischki T K, Lopinski G P and Wayner D D 2009 Evidence for initiation of thermal reactions of alkenes with hydrogen-terminated silicon by surface-catalyzed thermal decomposition of the reactant *Langmuir* **25** 5626–30
[19] Maboudian R, Ashurst W R and Carraro C 2000 Self-assembled monolayers as anti-stiction coatings for MEMS: characteristics and recent developments *Sensors Actuators* A **82** 219–23
[20] Luo J K, Fu Y Q, Le H R, Williams J A, Spearing S M and Milne W I 2007 Diamond and diamond-like carbon MEMS *J. Micromech. Microeng.* **17** S147–63
[21] Greiner C, Felts J R, Dai Z, King W P and Carpick R W 2012 Controlling nanoscale friction through the competition between capillary adsorption and thermally activated sliding *ACS Nano* **6** 4305–13
[22] van Spengen W M, Bakker E and Frenken J W M 2007 A 'nano-battering ram' for measuring surface forces: obtaining force–distance curves and sidewall stiction data with a MEMS device *J. Micromech. Microeng.* **17** S91–7
[23] Kokorian J, Buja F and van Spengen W M 2015 In-plane displacement detection with picometer accuracy on a conventional microscope *J. Microelectromech. Syst.* **24** 618–25
[24] Balavalad K B and Sheeparamatti B G 2015 A critical review of MEMS capacitive pressure sensors *Sensors Transducers* **187** 120–8
[25] Beechem T, Graham S, Kearney S P, Phinney L M and Serrano J R 2007 Simultaneous mapping of temperature and stress in microdevices using micro-Raman spectroscopy *Rev. Sci. Instrum.* **78** 061301
[26] Szoszkiewicz R and Riedo E 2005 Nucleation time of nanoscale water bridges *PRL* **95** 135502
[27] van Spengen W M, Turq V and Frenken J W M 2010 The description of friction of silicon MEMS with surface roughness: virtues and limitations of a stochastic Prandtl–Tomlinson model and the simulation of vibration-induced friction reduction *Beilstein J. Nanotechnol.* **1** 163–71
[28] van Spengen W M, Puers R and De Wolf I 2002 A physical model to predict stiction in MEMS *J. Micromech. Microeng.* **12** 702–13
[29] Tas N R 2000 Electrostatic micro walkers *PhD Thesis* University of Twente (p 74)
[30] Bhushan B and Li X 1997 Micromechanical and tribological characterization of doped single-crystal silicon and polysilicon films for microelectromechanical systems devices *J. Mater. Res.* **12** 54–63
[31] Plößl A and Kräuter G 1999 Wafer direct bonding: tailoring adhesion between brittle materials *Mater. Sci. Eng.* R **25** 1–88
[32] van Spengen W M 2015 A physical model to describe the distribution of adhesion strength in MEMS, or why one MEMS device sticks and another 'identical' one does not *J. Micromech. Microeng.* **25** 125012